LAWRENCE
LIVERMORE
NATIONAL
LABORATORY

LLNL-PROC-410671

Isochoric heating of reduced mass targets by ultra-intense laser produced relativistic electrons

P. Neumayer, H. J. Lee, D. Offerman, E. Shipton, A. Kemp, A. L. Kritcher, T. Doppner, C. A. Back, S. H. Glenzer

February 18, 2009

Radiative Properites of Hot Dense Matter
Santa Barbara, CA, United States
November 10, 2008 through November 14, 2008

Disclaimer

Isochoric heating of reduced mass targets by ultra-intense laser produced relativistic electrons

P. Neumayer[a], H. J. Lee[b], D. Offerman[c], E. Shipton[c], A. Kemp[a], A. L. Kritcher[b,a], T. Döppner[a], C. A. Back[d], S. H. Glenzer[a]

[a] *Lawrence Livermore National Laboratory, P.O. Box 808, Livermore, CA 94551, USA*
[b] *University of California, Berkeley, CA 94720, USA*
[c] *University of California, San Diego, La Jolla, California 92093, USA*
[d] *General Atomics, P.O. Box 85608, San Diego, California 92186, USA*

Abstract

We present measurements of the chlorine K-alpha emission from reduced mass targets, irradiated with ultra-high intensity laser pulses. Chlorinated plastic targets with diameters down to 50 micrometers and mass of a few 10^{-8} g were irradiated with up to 7 J of laser energy focused to intensities of several 10^{19} W/cm^2. The conversion of laser energy to K-alpha radiation is measured, as well as high resolution spectra that allow observation of line shifts, indicating isochoric heating of the target up to 18 eV. A zero-dimensional 2-temperature equilibration model, combined with electron impact K-shell ionization and post processed spectra from collisional radiative calculations reproduces the observed K-alpha yields and line shifts, and shows the importance of target expansion due to the hot electron pressure.

Key words: reduced mass target, isochoric heating, K-alpha, line shifts

1. Introduction

With the advent of high-energy high-intensity lasers [1] the field of ultra-intense laser-matter interaction has rapidly evolved and demonstrated a vast potential of technical applications, from the acceleration of electrons to high quality GeV beams [2], proton and heavy ion acceleration [3, 4], over high brightness x-ray sources for high-energy density plasma diagnostics such as spectrally resolved x-ray scattering [5, 6] to the fast ignition approach [7] to inertial confinement fusion [8]. However, the understanding of both the generation of electrons with MeV temperatures in the interaction of an ultra-high intensity laser pulse with matter, and their subsequent transport through and energy exchange with the target still pose a significant challenge to theory. Dimensions and time scales relevant to experiments typically exceed largely the available computing power. Therefore, well characterized experiments with small dimensions and simple geometries are required to allow comparison with extensive integrated calculations. Such experiments however may also allow comparison to simple models with strongly reduced complexity. This allows to identify the dominant/relevant processes and give more intuitive insight into the mechanisms at work.

Reduced mass targets, with dimensions of a hundred down to few 10's of micrometers, offer an interesting means to study the interaction of these relativistic electrons with the target. The range of the hot electrons typically exceeds the target dimensions, and refluxing due to self-induced electric sheath fields confines the hot electrons to the target. This process prolongs the interaction time with the bulk electrons of the target and has been proposed to create extremely high energy density states of matter, like solid density plasmas at keV temperatures, relevant to laboratory astrophysics [9]. Furthermore, micron sized targets are also employed to enhance the spatial resolution in point-projection x-ray radiography [10].

K-emission spectroscopy is a convenient means to diagnose plasmas with hot electrons, as K-shell radiation is naturally emitted following the electron impact K-shell ionization. Absorption lengths exceed the target dimensions, so that emission from the bulk target is diagnosed. K-alpha spectra from copper and titanium targets irradiated with several 100 J of laser energy indicated increased heating up to 200 eV when the target dimension were reduced to 100 micron [11, 12]. Nilson et al. [13] used the ratio of L-M to M-K shell radia-

tion to infer bulk temperatures of 200 eV in reduced-mass-targets, irradiated with only 10 J of laser energy. This ratio changes when the temperature is large enough (100 eV) to allow ionization of the target atoms into the M-shell, and thus is only sensitive to large temperatures.

In this paper we report on experiments measuring high-resolution spectra of the chlorine K-alpha emission from reduced-mass plastic targets, irradiated by ultra-intense laser pulses of a few Joule energy. Measuring spectral line shifts with an accuracy of $\lesssim 0.4$ eV enables us to detect temperature increases as small as a few eV. The data can be reproduced by calculations using a collisional 2-temperature model, describing the temperature equilibration between the hot electron fraction and the cold bulk electrons, coupled to spectra calculations using a collisional radiative code.

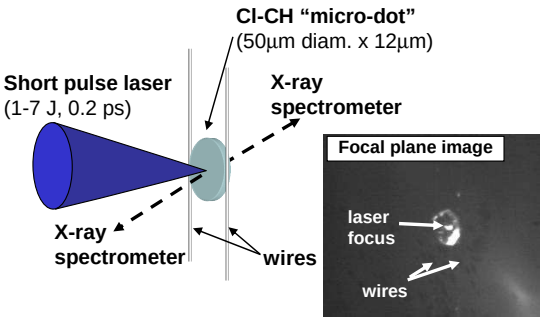

Figure 1: Schematic of the experimental configuation. The micro-dot targets (diameters 100 and 50 μm) are subtended by two 8 μm silicon fibers and are irradiated with ultra-high intensity laser pulses with energies up to several Joule. K-alpha emission from front and rear side of the target is detected by two efficient, high-resolution x-ray spectrometers. An in-situ microscope allows positioning and overlap of the target and the laser focus.

2. Experimental setup

The experiment was carried out at the Jupiter Laser Facility at the Lawrence Livermore National Laboratory (LLNL). Laser pulses with energies ranging between 1...7 J at pulse durations of ≈ 0.2 ps were focused on target with a F/2.2 off-axis parabola. The focal spot was imaged by a 40x microscope. The focal spot diameter was approximately 3 μm (FWHM), with about 40-50 % of the total pulse energy contained within the $1/e^2$ contour. The pre-pulse level was measured to be lower than 10^{-6} of the main pulse. The targets were made of Polyvinyldenchloride ("Saran", $C_7H_8Cl_3$). Round dots of 50 and 100 μm diameter were punched out of 12.5 micron thick foil and glued to two 8 micron silicon fibers. The targets were overcoated with a 1 μm thick CH tamper. This avoids chlorine ions in the blow-off plasma, ensuring that K-shell emission is coming from the solid density material, with a negligible effect on the K-alpha yield [14].

Both laser focus and target were positioned and overlapped in the target chamber using an in-situ camera microscope. Fig. 1 shows an image of an aligned 50 μm diameter target and the focal spot produced by the laser oscillator. An alignment wire (15 μm diameter) could be driven into the focus and served as a reference to allow reproducible positioning of the targets to $\lesssim 50\mu$m. Longitudinal positioning of the targets to $\lesssim 50\mu$m was aided by a side-on imaging setup at 10x magnification. Large ($\approx$ mm) size foils of the same target material were shot as reference.

Spectra of the K-alpha line emission of chlorine at photon energies ≈ 2.6 keV were measured by two x-ray spectrometers viewing the front (i.e. where the laser is incident) and the rear side of the target. The spectrometers employed flat HOPG (highly-oriented pyrolytic graphite) crystals in para-focusing geometry [15, 16]. The HOPG lattice spacing of 3.35 Å only allowed the crystals to be used in 1st diffraction order. However, by using a large spectrometer arm length of 40 cm a dispersion of 3.7 eV/mm could be achieved. This high dispersion was required to limit the influence of thermal and mechanical drifts on the spectral accuracy of the setup. The two spectrometers were set up such that a shift of the source location would show up as a red-shift in one and a blue-shift in the other spectrometer. This way a spectral shift could easily be distinguished from a shift caused by misalignment of the target. The spectrally resolved radiation was recorded on imaging plates (BAS-TR type, Fujifilm). The cassette to hold the imaging plates was designed to allow repositioning with an accuracy of better than 100 μm. Given the spectrometer dispersion this results in a shot-to-shot reproducibility of the spectral position of $\lesssim 0.4$ eV. We estimate the resolution limit of the spectrometer to 0.6 eV. This includes broadening due to the finite source size (0.4 eV), detector resolution (0.4 eV), roughness, depth and intrinsic broadening (0.3, 0.1, 0.3 eV, respectively), and aberration broadening due to the flat crystal used (0.1 eV) [15]. To enable absolute measurements of the x-ray emission the response of the imaging plates was calibrated against an absolutely calibrated CCD camera [17].

3. Modeling

In the interaction of an ultra-intense laser pulse with matter, copious amounts of high-energy electrons with

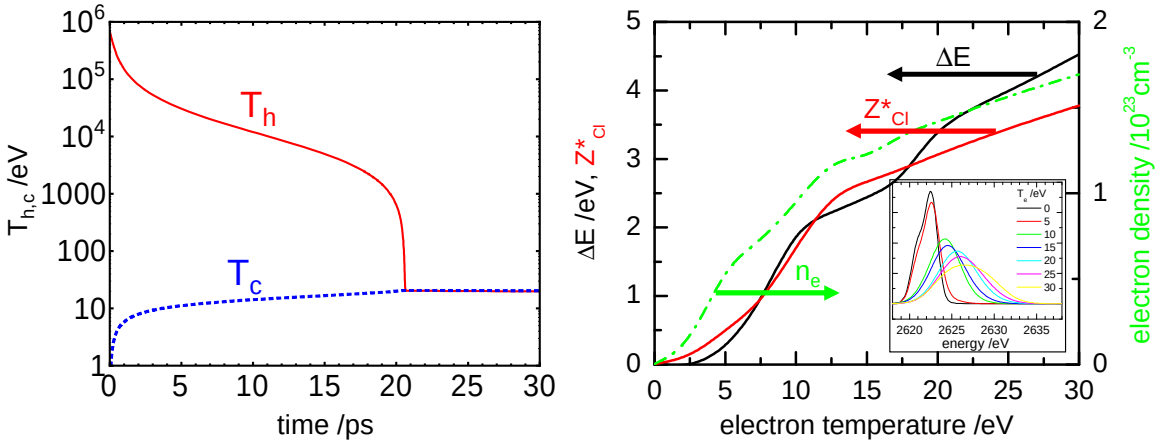

Figure 2: (left) Temperature evolution of the cold and hot electron population, calculated by the model described in the text. (right) Chlorine charge state $Z^*_{\rm Cl}$, electron density and spectral shift ΔE of the Cl-$K\alpha$ emission increase with increasing bulk temperature. The inset shows synthetic Cl-$K\alpha$ spectra for electron temperatures $0 \le T_{\rm e} \le 30$ eV. Ionization balance and spectra calculations are performed by FLYCHK.

typical energies of MeV are produced. These relativistic electrons have ranges of several 100 μm in the target, largely exceeding the dimensions of our targets. They are reflected at the target surfaces by self-induced sheath fields [18]. For a simple model we therefore assume a homogenous hot electron density confined to the dimensions of the target.

We employ the 2-temperature collisional equilibration model discussed in [19] to interprete our experimental results. Hot electrons generated by the intense laser pulse instantaneously spread over the entire target and exchange energy with the remaining (cold) bulk electrons via collisions at a collision frequency $\nu_\epsilon^{hc} = \frac{8\sqrt{2\pi}e^4}{3\sqrt{m_e}} \frac{n_{e,c}\ln\Lambda}{(k_B T_c + k_B T_h)^{3/2}}$ and $\nu_\epsilon^{ch} = \frac{n_{e,h}}{n_{e,c}}\nu_\epsilon^{hc}$. Here $n_{e,c}$ ($n_{e,h}$) are the densities of the cold (hot) electron fraction, e and m_e the electron charge and mass, and k_B is Boltzmann's constant. We used a Coulomb logarithm of $\Lambda = 5$. In addition, the hot electron fraction cools adiabatically due to expansion, according to $pV^\gamma = $ const. with the adiabatic coefficient $\gamma = 5/3$. We use the analytical expression from [20] for the expansion velocity of the ion front into vacuum

$$L'(t) = 2\,c_s(t)(2\ln(\Omega_i t + 1) + \ln(2) - 1) \qquad (1)$$

with the ion sound velocity $c_s(t) = \sqrt{T_h(t)/M_i}$ and plasma frequency $\Omega_i = \sqrt{4\pi n_i Z_i^2 e^2/M_i}$ of the ions with mass M_i, average charge Z_i and density n_i.

With T_h (T_c) being the temperature of the hot (cold) electron fraction the temperature equilibration is then described by

$$T_h'(t) = \left(\frac{L_0}{L(t)}\right)^d \nu_\epsilon^{hc}\,(T_c(t) - T_h(t)) + \qquad (2)$$
$$+ \; d\,(1-\gamma)\,T_{h,0}\left(\frac{L_0}{L(t)}\right)^{(d(\gamma-1)+1)} L'(t)/L_0$$

$$T_c'(t) = \left(\frac{L_0}{L(t)}\right)^d \nu_\epsilon^{ch}\,(T_h(t) - T_c(t))\,. \qquad (3)$$

L_0 is the initial size of the target and d reflects the geometry of the expansion (1=planar, 3=spherical). The term $(L_0/L(t))^d$ in eq. 3 accounts for the decrease in density of the hot electron fraction as the ion front expands, while in eq. 2 it is the fraction of time the expanded hot electrons spend within the unexpanded cold electron population.

The initial hot electron density is $n_h(0) = N_h/V_0$ with the initial target volume V_0 and the number of hot electrons N_h. With the total energy of the hot electron fraction $E_{\rm hots}$ we obtain N_h from $E_{\rm hots} = N_h \int_0^\infty f(E;T_h)E{\rm d}E$, where $f(E;T_h)$ is the 3-dimensional relativistic distribution function at temperature T_h [21]. For the conversion of laser energy $E_{\rm laser}$ to hot electrons $E_{\rm hots} = \eta E_{\rm laser}$ we use an empirical fit to the absorption data by Y. Ping et al. [22] of $\eta = 0.6 \times 0.31(I_{18})^{0.15}$, where I_{18} is the focused laser intensity in units of 10^{18} W/cm^2, and assuming that 60% of the absorbed energy goes into hot electrons. The hot electron temperature T_h for a given laser intensity is obtained from the empirical scaling by Beg et al. [23].

An example for the temperature evolution of the cold and hot electron fraction is shown in Fig. 2. The param-

eters used in the calculation were $E_{\rm laser} = 6.5\,$J, $d = 2$, $L_0 = 50\,\mu$m and $I_{18} = 25$. Over the first 5 ps we see a rapid decrease of the hot electron temperature from $\approx$ 1MeV by almost two orders of magnitude. This decrease is entirely due to adiabatic cooling. The collisional cooling rate is 2 orders of magnitude lower at the high temperatures, as the scattering cross section and consequently ν_ϵ scales as $T^{-3/2}$. As the target expands and the hot electron pressure decreases, the adiabatic cooling rate slows down quickly. The collisional cooling rate stays approximately constant, as the decrease in density is balanced by the increasing collision rate. After $\gtrsim 15\,$ps the collisional cooling rate becomes comparable and T_h and T_c quickly equilibrate, in this example after about 20 ps.

The total K-alpha yield is obtained from $\int \Phi_{\rm K\alpha}(t)$dt with the K-alpha emission rate

$$\Phi_{\rm K_\alpha}(t) = \eta_{\rm K_\alpha} N_{e,h} n_{i,\rm Cl} \int_0^\infty \sigma_K(E) v(E) f(E;T) {\rm dE}. \quad (4)$$

Here $v(E)$ is the electron velocity at the (relativistic) energy E, $n_{i,\rm Cl}$ is the density of the chlorine ions in the target and $\eta_{\rm K\alpha} = 0.1$ is the K-alpha fluorescence yield. For the K-shell ionization cross section by electron impact, σ_K, we use the empirical expression by Hombourger [24], which includes the relativistic increase for electron energies above 0.5 MeV. For typical conditions, the resulting chlorine K-shell ionization rate is of order $10^{25}{\rm s}^{-1}$. The total number of chlorine ions $n_{i,\rm Cl} V_0$ is of order 10^{15} ions, so the average K-shell ionization rate is $\approx 10^{10}{\rm s}^{-1}$ per ion. This is significantly lower than the K-vacancy decay rate which is $\approx 10^{14}{\rm s}^{-1}$ [25], justifying eq. 4 which implies that no significant depopulation takes place and the emission rate is limited only by the K-shell ionizations rate.

Synthetic K-alpha spectra are generated by post-processing the electron temperature evolution obtained from the equilibration model with steady state emission spectra calculated by FLYCHK [26]. FLYCHK is a collision-radiative kinetics code which includes high-density effects like continuum-lowering and pressure ionization as well as the effects of a hot electron fraction.

Figure 2 (right) shows the shift ΔE of the K-alpha peak for bulk electron temperatures $T_c = 0...30\,$eV. This line shift is a result of the increasing charge state $Z^*_{\rm Cl}$ of the chlorine ions, with increasing temperature. Besides the electron temperature, the background electron density has a non-negligible effect on the ionization dynamics and on the achieved charge state. At low temperatures, higher densities result in more pressure ionization, and an increased charge state. At higher temperatures, pressure ionization becomes less important, while increased 3-body recombination lowers the charge state. We calculate the electron density from a self-consistent solution for the average charge states of the different ion species within the target, where the density dependent charge states for each species is obtained from FLYCHK. The inset in Fig. 2 shows the actual spectra computed by FLYCHK.

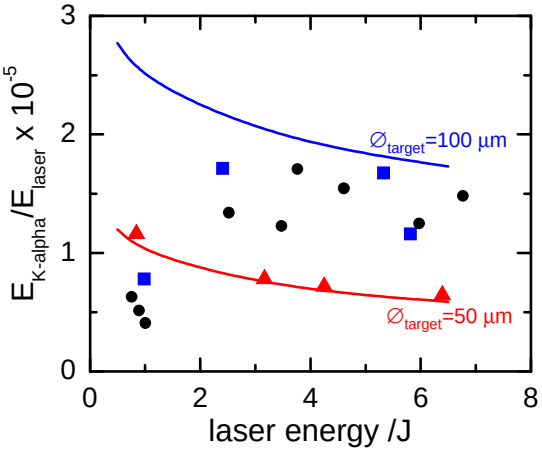

Figure 3: Conversion efficiency of laser energy into Cl K-alpha radiation for 100μm (blue squares), 50μm (red triangles) diameter, and foil targets (black dots). Also shown is the calculated conversion efficiency using the model (solid lines).

4. Results and discussion

4.1. Conversion efficiency

Figure 3 shows the total yield of K-alpha radiation (into 4π sr), normalized to the incident laser energy, i.e. the conversion efficiency. The absolute error of the measurement is dominated by the uncertainty of the quantum efficiency $\eta_{\rm CCD}$ of the CCD camera, used for the calibration of the image plate response, and the integrated reflectivity $R_{\rm HOPG}$ of the spectrometer crystal. We used the factory specified $\eta_{\rm CCD} = 0.96$ [17] and a $R_{\rm HOPG} = 0.003\,$rad as measured in [27], and estimate the combined error to $\approx$ 50%. Uncertainty due to filter thickness is estimated to 5% as only 50 μm of Beryllium were used. The relative error of the measurement is of order 1% due to the calorimeter shot-to-shot repeatability. The error due to photon statistics is negligible, as several 10^4 photons are detected per shot.

The conversion efficiencies obtained in these experiments are typically of order $E_{\rm K\alpha}/E_{\rm laser} \approx 10^{-5}$, consistent with previous experiments [28]. The larger, 100μm diameter targets reach the same values as foil targets,

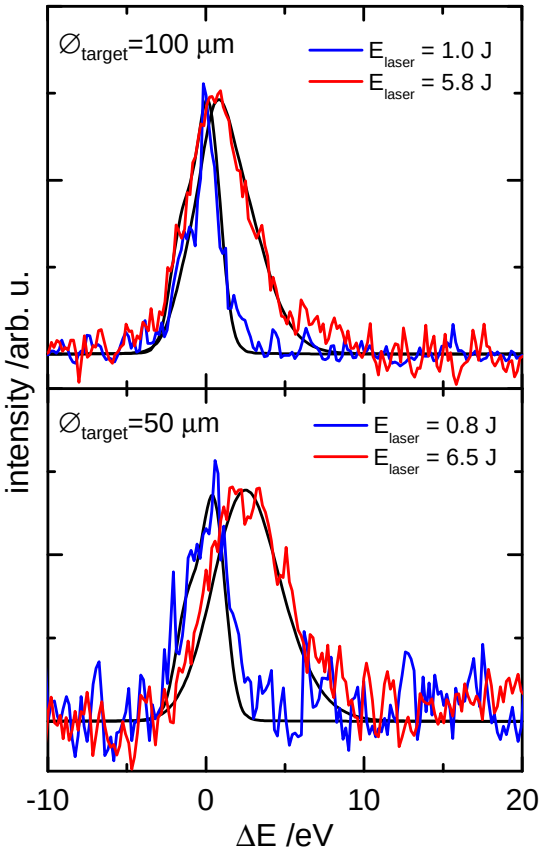

Figure 4: Typical K-alpha emission spectra from from a 100 μm (top) and a 50 μm (bottom) diameter target, for different laser energies. The broadening and shift towards higher photon energies indicates an increased bulk electron temperature. Also shown are synthetic spectra as obtained from the temperature equilibration model combined with spectra calculated by FLYCHK (see text).

whereas conversion efficiencies from the smaller, 50μm diameter targets are about 1.5−2× lower. Also shown in Fig. 3 are calculations from our model. While a planar expansion ($d = 1$) was assumed for the 100 μm diameter targets, for the smaller, 50 μm targets, $d = 2$ yielded a better agreement with the measured conversion efficiencies. The 2D expansion results in a faster adiabatic cooling and equilibration of the hot electron fraction which explains the observed reduction in K-alpha yield. This is consistent with the choice of d for the calculation of the spectral shifts (see below). The slightly decreasing trend with increasing laser energy is due to the larger initial T_h which results in a faster target expansion.

4.2. Spectral shifts

Figure 4 shows typical spectra of the K-alpha emission, for 100 μm and 50 μm diameter targets, shot with low ($E_{\mathrm{laser}} \lesssim 1$ J) and high (≈ 6 J) laser energies. The energy shift ΔE is given relative to the center of the spectral line of the lower energy shot. For the higher energy shots we observe a significant blue shift of the line emission, for the smaller targets by up to 3 eV. At the same time, the line width increases from 6 eV (FWHM) to 9 eV for the larger targets and to 12 eV for the smaller targets. As seen from the FLYCHK calculations (fig. 2) a line shift of 3 eV corresponds to a chlorine charge state $Z^*_{\mathrm{Cl}} \approx 3$, as a consequence of a higher bulk electron temperature of about $T_c \approx 18$ eV.

The contribution of the prepulse to the temperature increase is expected to be negligible. We estimate it using the Hugoniot equation for the increase in internal energy in a single strong shock, $\Delta\epsilon = \frac{1}{2}(p_1 + p_0)(V_0 - V_1)$ [29], where $p_{0,1}$ and $V_{0,1}$ are the pressure and specific volume of the unperturbed and the shocked target, respectively. In the limit of a strong shock $p_1 \gg p_0$ and $\frac{V_0}{V_1} \approx \frac{\gamma+1}{\gamma-1} = 4$. The laser ablation pressure is obtained from scaling laws from [30]. At a prepulse intensity of 2.5×10^{13} W/cm^2 we estimate $p_1 \approx 4$ Mbar, resulting in an energy density of 100 MJ/kg. According to the Sesame equation of state for Polystyrene, this corresponds to a temperature of only 2.4 eV. This estimate is an upper bound, as 3D effects are not accounted for which would significantly lower the temperature. Also, the area of the focal spot covers only a few percent of the target face, and most of the target will be exposed to orders of magnitude lower intensities.

We therefore attribute the increased target temperature to the collisional energy transfer from the hot electron fraction to the cold bulk electrons. Attempting to reproduce the measured spectra directly by weighting the steady state spectra calculated by FLYCHK with the temperature history from our model did not yield a satisfactory agreement. The calculated K-alpha emission rate $\Phi_{\mathrm{K}\alpha}$ is strongest at $t = 0$, when the hot electron density is highest. The bulk electron temperature, however, starts out at $T_c = 0$ eV and rises to its final value over 10-20 ps. The simulated spectra therefore always show a strong contribution from cold material (i.e. $T_c \lesssim 5$eV) and only a weak tail towards higher energies, in disagreement with the experimentally observed blue shift of the entire line. This suggests that the temporal evolution of K-alpha emission is not well enough modeled here and more subtle effects, such as an increasing hot electron density due to secondary M-shell ionization, as suggested in [19], might play an important role. We therefore use the K-alpha time history as measured in [19] to weight the relative contributions from the different T_c. Figure 4 shows the simulated spectra, calculated

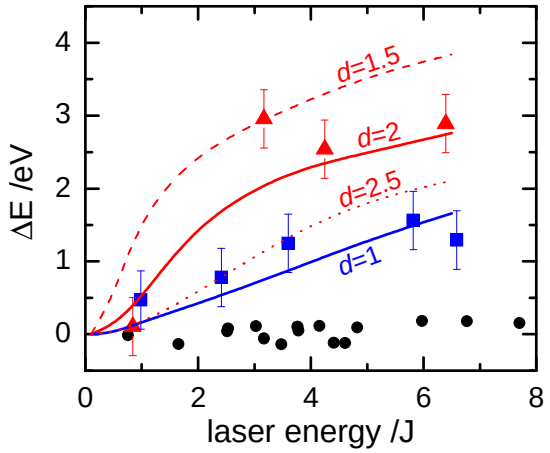

Figure 5: Relative shift of the center-of-gravity of the K-alpha emission with laser energy. The 50 μm diameter targets (red triangles) show larger line shifts than the larger, 100 μm diameter targets (blue squares). For the large, mm-size targets (black circle), $\Delta E \lesssim 0.3$ eV for all laser energies and demonstrates the shot-to-shot stability and accuracy of the relative shift measurement. The solid lines show model calculations, for various values of the dimension parameter d (see text).

for the corresponding experimental parameters. Both the shift and the line broadening are well reproduced by the synthetic spectra.

The relative shift of the Cl-$K\alpha$ line center-of-gravity as function of laser energy is shown in Fig. 5. Shifts of up to 1.5 eV and 3 eV are observed for the 100 μm and the 50 μm diameter targets, respectively. For the mm-size foil targets, the shifts are $\Delta E \lesssim 0.3$ eV, i.e. below the experimental accuracy, for all laser energies shot in this experiment, in good agreement with previous results [31]. Also shown in fig. 5 is the line shift calculated by our model. For the larger targets, the calculations reproduce the shift measured in the experiment, assuming a planar expansion of the target ($d = 1$). For the smaller targets, using $d = 1$ overestimates the shift. Better agreement is obtained with $d \approx 2$, indicating that the assumption of a planar expansion is less appropriate for the small targets. We note that for all simulations the hot electron temperature scaling by Beg et al. [23] was used. Using the ponderomotive scaling by Wilks et al. [32] the observed shifts could not be reproduced. This is because at the intensities used in this experiment, the ponderomotive scaling predicts significantly higher electron temperatures. As a consequence, both the collision rate and the hot electron density are smaller, resulting in a significantly slower energy transfer to the bulk electron system.

5. Conclusions

To summarize, we have measured the chlorine K-alpha emission from reduced mass targets of sizes down to 50 micron diameter, irradiated with high-intensity laser pulses of energies up to $\approx$ 7 J. Conversion of laser energy into K-alpha radiation on the order of 10^{-5} was obtained, with a reduction of 1.5-2 for the smallest targets. High resolution spectra revealed spectral line shifts by up to 3 eV to higher photon energies. Comparison of the data to calculations with a two temperature equilibration model show good agreement with both the conversion efficiency and the observed spectral shifts. The model includes collisional energy transfer, adiabatic cooling due to target expansion, and K-alpha generation, coupled to synthetic spectra generated using the collisional radiative code FLYCHK. The spectral shifts indicate target heating of up to $T_c \approx 18$ eV. We find that the data from the larger diameter targets are reproduced assuming a 1-dimensional expansion, while data from the smaller, 50 μm diameter targets suggests that 3D effects become important, resulting in a faster equilibration and reduced coupling to the bulk electrons. This shows the important effect of the rapid expansion of the target interface into vacuum due to the hot electron pressure.

Acknowledgments

We would like to thank the staff of the Jupiter Laser Facility for their support. This work was performed under the auspices of the U.S. Department of Energy by the Lawrence Livermore National Laboratory, through the Institute for Laser Science and Applications, under contract DE-AC52-07NA27344. The authors also acknowledge support from Laboratory Directed Research and Development Grants No. 08-LW-004 and 08-ERI-002.

References

[1] Mourou et al., xxx **322**, 69 (1985). Backus et al.
[2] Geddes et al., xxx **322**, 69 (2008).
[3] M. Roth et al., xxx **322**, 69 (2008).
[4] M. Hegelich et al., xxx **322**, 69 (2008).
[5] A. L. Kritcher, P. Neumayer, J. Castor et al., Science **322**, 69 (2008).
[6] S. H. Glenzer and R. Redmer, Rev. Mod. Phys. **xx**, xx (200x).
[7] Tabak et al., xxx **322**, 69 (2008).
[8] Lindl et al., xxx **322**, 69 (2008).
[9] B. A. Remington, R. P. Drake, and D. D. Ryutov, Rev. Mod. Phys. **78**, 755 (2006).
[10] H.-S. Park et al., xxx **322**, 69 (2008).
[11] G. Gregori, S. B. Hansen, R. Clarke et al., Contrib. Plasma Phys. **45**, 284 (2005).

[12] S. N. Chen, G. Gregori, P. K. Patel et al., Phys. Plasmas **14**, 102701 (2007).
[13] P. M. Nilson, W. Theobald, J. Myatt et al., Phys. Plasmas **15**, 056308 (2008).
[14] A. L. Kritcher, P. Neumayer, M. K. Urry et al., xxx
[15] G. E. Ice and C. J. Sparks, NIM A **291**, 110 (1990).
[16] A. Pak, G. Gregori, J. Knight et al., Rev. Scient. Instrum. **75**, 3747 (2004).
[17] Andor Technologies, Model DX 420-BN.
[18] Y. Sentoku, T. E. Cowan, A. Kemp, and H. Ruhl, Phys. Plasmas **10**, 2009 (2003).
[19] H. Chen, R. Shepherd, H. K. Chung, et al., Phys. Rev. E **76**, 056402 (2007).
[20] P. Mora, Phys. Rev. Lett., **90** 185002 (2003).
[21] F. Ewald, H. Schwoerer and R. Sauerbrey, Europhys. Lett., **60** 710 (2002).
[22] Y. Ping, R. Shepherd, B. F. Lasinski et al., Phys. Rev. Lett. **100** 085004 (2008).
[23] F. N. Beg, A. R. Bell, A. E. Dangor et al., Phys. Plasmas **4** 447 (1997).
[24] C. Hombourger, J. Phys. B **31** 3693 (1998).
[25] J. H. Scofield, Phys. Rev. A **9**, 1041 (1974).
[26] H.-K. Chung, M.H. Chen, W.L. Morgan et al., HEDP **1** 3 (2005).
[27] F. J. Marschall and J. A. Oertel, Rev. Sci. Instrum. **68** 735 (1997).
[28] M.K. Urry, G. Gregori, O.L. Landen et al., J. Quant. Spectr. Rad. Trans. **99** 636 (2006).
[29] Y. B. Zel'dovich and Y. P. Raizer, *Physics of Shock Waves and High-Temperature Hydrodynamic Phenomena*, Academic Press (1966).
[30] D. Batani, H. Stabile, A. Ravasio et al., Phys. Rev. E **68** 067403 (2003).
[31] A. Sengebusch, S. H. Glenzer, A. L. Kritcher et al., Contrib. Plasma Phys. **47**, 309 (2007).
[32] S. C. Wilks, W. L. Kruer, M. Tabak, and A. B. Langdon, Phys. Rev. Lett. **69** 1383 (1992).